Optimization and Dynamic Modeling of Galfenol Unimorphs

LIANG SHU,[1,2] MARCELO J. DAPINO,[2,*] PHILLIP G. EVANS,[2] DINGFANG CHEN[1] AND QUANGUO LU[1,3]

[1]*Institute of Intelligent Manufacturing and Control, Wuhan University of Technology, Wuhan 430063, China*

[2]*Department of Mechanical and Aerospace Engineering, The Ohio State University, Columbus, OH 43210, USA*

[3]*Institute of Micro/Nano Actuation and Control, Nanchang Institute of Technology, Nanchang 330099, China*

ABSTRACT: Design and modeling of a bi-laminate, Galfenol-driven composite beam is presented in which the elasticity of the adhesive layer is considered. The optimal thickness ratio necessary to maximize the tip deflection is found by minimization of the internal energy of the beam. Model simulations show that use of a substrate material with high modulus leads to larger tip deflections. Stainless steel was therefore utilized as substrate in the experiments. In order to reduce eddy currents, a laminated silicon steel frame was employed to magnetize the beam. A dynamic model is proposed by coupling the structural dynamics of the beam and adhesive layer with the magnetostriction generated by the Galfenol layer. The latter is described with a linear piezomagnetic law with uniform magnetic field distribution along the length of the beam. Galerkin discretization combined with Newmark numerical integration are employed to approximate the dynamic response of the beam. The model is shown to describe both the transient and steady-state response of the composite beam tip displacement under harmonic excitation between 10 and 320 Hz. The RMS error between model and data range between 1.44% at 10 Hz and 6.34% at 320 Hz, when the same set of model parameters (optimized at quasistatic frequency) is utilized.

Key Words: magnetostrictive unimorph, Galfenol, dynamic model.

INTRODUCTION

GALFENOL is a recent magnetostrictive material which exhibits moderately high magnetically induced strain and intrinsic steel-like structural properties (Evans and Dapino, 2008). Unlike most active materials, Galfenol is suitable for load-carrying transducers operating under combined loads.

At present, most active laminated structures take advantage of piezoelectric materials or the giant magnetostrictive material Terfenol-D (Krishnamurthy, 1999; Kumar et al., 2003). Zabihollah et al. (2007) presented a laminated structure for vibration suppression. Piezoceramic and PVDF patches were respectively used as the actuation and sensing elements, and a linear quadratic regulator controller was designed to suppress the vibrations of the composite beam. Suhariyono et al. (2008) presented a lightweight piezo-composite actuator (LIPCA) which achieves 41% higher actuation moment than bare PZT. Despite this improvement, piezoelectric materials are too brittle and cannot withstand large bending or tensile loads (Baillargeon and Vel, 2005). This limitation can be partially addressed through the use of thin patches with small surface areas, at the expense of actuation authority. One approach for avoiding premature failure is the use of piezoelectric shear actuators embedded within sandwich beams (Sun and Zhang, 1995; Baillargeon and Vel, 2005). Another way to design active laminated structures is using active thin film. Chen (2004) presented a MEMS microswitch with piezoelectric-film actuation and proposed a mathematical model which accounts for normal and shear stresses. Lee and Cho (2008) investigated a multilayer deposition technique of thin film for fabrication of a magnetostrictive actuator.

Galfenol has been utilized in active structures such as micro-actuators (Ueno and Higuchi, 2007), MEMS devices (Basantkumar et al., 2006), and laminated sensors (Downey and Flatau, 2005; Datta et al., 2008). Ueno and Higuchi (2007) investigated a micro-bending actuator based on Galfenol. A Galfenol C-shaped yoke was bonded with stainless steel plates, in which the yoke was machined from a plate of 1 mm thick polycrystalline Galfenol. The first resonance frequency is 1.6 kHz and it was shown that the actuator could withstand a suspended weight of 500 g. Downey and Flatau (2005) investigated the magnetoelastic bending of Galfenol for sensor applications. A series of experiments were conducted under dynamic bending loads to facilitate design concepts.

*Author to whom correspondence should be addressed.
Email: dapino.1@osu.edu
Figures 3, 4 and 7–11 appear in color online: http://jim.sagepub.com

1045-389X/11/08 0781–13 $10.00/0 DOI: 10.1177/1045389X11403822

Such applications motivate the development of a modeling framework for active laminated structures. Structural modeling of extensional magnetostrictive transducers has successfully been performed (Dapino et al., 2000), while the structural modeling of active laminated structures in bending has been a challenge.

Datta et al. (2008) have developed a magnetomechanical model for sensors in laminated structures. This model can be used to analyze the response of the active Galfenol layer to quasi-static axial and shear force and bending moments. Wang et al. (2010) presented a Galfenol layer bonded to a PZT-5H layer. It was found that a decrease in the thickness of the piezoelectric layer led to an increase in the tip deflection and greater charge generation by the PZT layer. An actuation model was proposed by Datta et al. (2009) to predict magnetostrictive strains and stresses in laminated plates under quasi-static magnetic fields. The contribution of their study was the combination of the magnetomechanical material model and the structural plate model. However, the adhesive layer was not considered in their study. Bashash et al. (2009) presented another hysteresis model based on recursive memory. A Galfenol-driven micropositioning actuator and a piezoelectrically driven nanopositioning stage were used to experimentally validate the model in the static domain. du Trémolet de Lacheisserie and Peuzin (1994) investigated deformations of a bimorph actuator consisting of a non-magnetic substrate and a magnetic thin film. Their model is suitable for a very thin film deposited on a non-magnetic substrate. The film thickness was assumed to be far less than the substrate thickness so that the mechanical energy in the active layer could be taken as constant since internal stress in the film hardly changes through the thickness. Models for any thickness ratio have been presented by Gehring et al. (2000) and Guerrero and Wetherhold (2003) based on total internal energy minimization. Since the cantilevers discussed were made of active film deposited on a non-magnetic substrate, no adhesive layer was included.

Yan et al. (2009) developed an analytical expression for the static behavior of surface-bonded piezoelectric transducers, in which the interfacial shear stresses between the piezoelectric patches and the host elastic beam were considered. Numerical calculations showed that the actuation authority of the piezoelectric patches decreases for thicker adhesive layers. The effect of piezoactuator thickness on the active vibration control of a cantilever beam was investigated by Kim and Jones (1995). The analytical solution of the deflection was derived from Euler's beam equation. The effect of the bonding layer thickness was investigated by assuming the excitation frequency was zero. In the Euler beam equation, the structural damping was assumed to be zero and no experiment was implemented to verify the effect of the bonding layer.

This article investigates the dynamic response of Galfenol-driven laminated beam actuators considering the effect of the substrate and adhesive layer on tip displacement. A U-shaped frame was designed and fabricated to excite the beam with dynamic magnetic fields. In order to reduce eddy current losses in the frame, laminated silicon steel was utilized. We present a dynamic Galfenol-driven composite beam model, in which the Galfenol layer is bonded to a non-magnetic substrate. The energy loss or damping from the adhesive layer is considered as is the stress variaration through the Galfenol thickness. Experiments and simulations are conducted to study the influence of thickness ratio and material parameters on tip displacement. The optimal design of a composite beam micro-positioner is discussed first, followed by a dynamic model which combines the piezomagnetic constitutive law and the structural beam model. The experiments and results are presented next, followed by concluding remarks.

OPTIMAL BEAM DESIGN

The composite beam, consisting of a Galfenol layer bonded to a non-magnetic substrate, is clamped at one end while the other end is free (Figure 1). The length of the beam is L and the width is b. The xy plane of the coordinate system is set on the neutral plane of the cantilever and the z axis is perpendicular to the active layer plane. Euler beam assumptions are employed. The out-of-plane strain is negligible since the in-plane dimensions of the beam are large relative to its thickness. The Poisson's ratio of the materials is not taken into

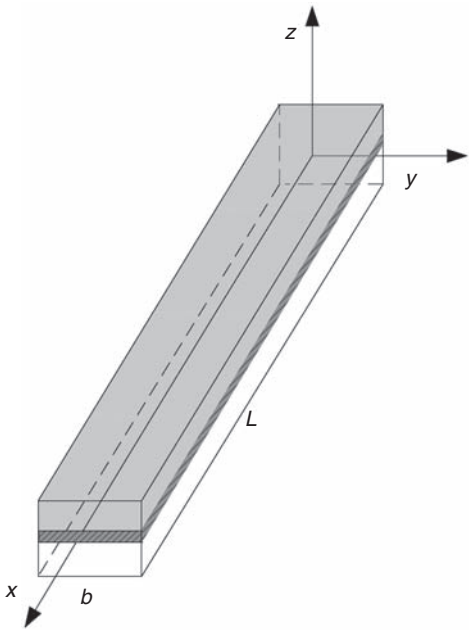

Figure 1. *Coordinate system of the cantilever.*

account since the length of the beam is much greater than the width.

The thickness of the composite beam is t; the subscripts g, s, and m are used to denote the Galfenol layer, substrate layer, and adhesive layer, respectively (Figure 2). The distance from the top of the beam to the neutral axis is h.

For the adhesive and substrate layers, there is no magnetostriction and the stress in the layers is assumed to follow Hooke's law. The total axial strain of the Galfenol layer is the sum of the purely elastic strain obeying Hooke's law and the magnetostriction:

$$\epsilon_x = \frac{\sigma_g}{E_g} + \lambda, \tag{1}$$

and thus the stress is:

$$\sigma_g = E_g(\epsilon_x - \lambda), \tag{2}$$

where E represents Young's modulus (with subscript g, s, or m) and λ denotes magnetostriction. The axial strain at any point in the composite can be expressed as

$$\epsilon_x = -\kappa z, \tag{3}$$

where κ is the curvature of the beam. The x-axis normal stress in each layer thus has the form

$$\begin{aligned} \sigma_g &= -E_g(\kappa z + \lambda), \\ \sigma_s &= -E_s \kappa z, \\ \sigma_m &= -E_m \kappa z. \end{aligned} \tag{4}$$

The total energy of the beam is calculated by integrating the sum of the energy densities of each layer over the beam volume:

$$\begin{aligned} U =& \int_V \frac{1}{2} E_s(\kappa z)^2 \mathrm{d}V + \int_V \frac{1}{2} E_m(\kappa z)^2 \mathrm{d}V + \int_V \frac{1}{2} E_g(\kappa z + \lambda)^2 \mathrm{d}V \\ =& \int_{h-t_s-t_g-t_m}^{h-t_g-t_m} \mathrm{d}z \int_0^b \mathrm{d}y \int_0^L \frac{1}{2} E_s \kappa^2 z^2 \mathrm{d}x \\ &+ \int_{h-t_g-t_m}^{h-t_g} \mathrm{d}z \int_0^b \mathrm{d}y \int_0^L \frac{1}{2} E_m \kappa^2 z^2 \mathrm{d}x \\ &+ \int_{h-t_g}^{h} \mathrm{d}z \int_0^b \mathrm{d}y \int_0^L \frac{1}{2} E_g(\kappa z + \lambda)^2 \mathrm{d}x \\ =& \frac{E_s \kappa^2 bL}{6}[(h - t_g - t_m)^3 - (h - t_g - t_m - t_s)^3] \\ &+ \frac{E_m \kappa^2 bL}{6}[(h - t_g)^3 - (h - t_g - t_m)^3] \\ &+ \frac{E_g \kappa^2 bL}{6}[h^3 - (h - t_g)^3] - \frac{1}{2} E_g bL \kappa \lambda [h^2 - (h - t_g)^2] \\ &+ \frac{1}{2} \lambda^2 E_g t_g bL. \end{aligned} \tag{5}$$

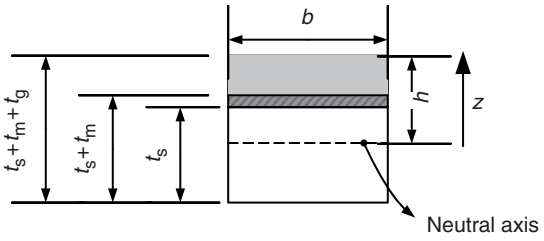

Figure 2. *Geometry of the thickness and neutral axis.*

The neutral axis is found by setting the x-axis force equal to zero:

$$\begin{aligned} F(h) =& \int_{A_s} \sigma_s \mathrm{d}A_s + \int_{A_m} \sigma_m \mathrm{d}A_m + \int_{A_g} \sigma_g \mathrm{d}A_g \\ =& -E_s \int_{h-t_g-t_s-t_m}^{h-t_g-t_m} \mathrm{d}z \int_0^b (\kappa z)\mathrm{d}y \\ &- E_m \int_{h-t_g-t_m}^{h-t_g} \mathrm{d}z \int_0^b (\kappa z)\mathrm{d}y \\ &- E_g \int_{h-t_g}^{h} \mathrm{d}z \int_0^b (\kappa z + \lambda)\mathrm{d}y \\ =& -\frac{1}{2} E_s \kappa b(2t_s(h - t_g - t_m) - t_s^2) - E_g b t_g \lambda \\ &- \frac{1}{2} E_m \kappa b(2t_m(h - t_g) - t_m^2) - \frac{1}{2} E_g \kappa b(2ht_g - t_g^2) \\ =& 0. \end{aligned} \tag{6}$$

Collecting h terms in (6) one obtains:

$$\begin{aligned} (E_s t_s + E_m t_m + E_g t_g)h =& \frac{1}{2}(E_s t_s^2 + E_m t_m^2 + E_g t_g^2) \\ &+ E_m t_m t_g + E_s t_s(t_g + t_m) - \frac{E_g t_g}{\kappa}\lambda. \end{aligned} \tag{7}$$

Since the maximum deflection of the laminated beam is of interest, the magnetostriction λ can be taken as the saturation value λ_s. With the definition of the following constants:

$$\begin{aligned} \tilde{B} &\equiv E_s t_s^2 + E_m t_m^2 + E_g t_g^2, \\ \tilde{A} &\equiv E_s t_s + E_m t_m + E_g t_g, \end{aligned} \tag{8}$$

the location of the neuatral axis with respect to the top of the beam can be expressed in terms of curvature κ as

$$h = \frac{1}{2}\frac{\tilde{B}}{\tilde{A}} + \frac{E_m t_m t_g}{\tilde{A}} + \frac{E_s t_s(t_g + t_m)}{\tilde{A}} - \frac{E_g t_g \lambda_s}{\tilde{A}}\frac{1}{\kappa}. \tag{9}$$

Substitution of (9) into (5) gives the total energy as a function of κ. Energy minimization with respect to κ yields

$$\kappa = -\frac{6\lambda_s \Theta}{E_g^2 t_g^4 + 4\Phi + 6\Psi + 12\delta t + E_m^2 t_m^4 + E_s^2 t_s^4}, \tag{10}$$

where

$$\begin{aligned}
&\alpha = E_g E_m t_g t_m, \quad \beta = E_g E_s t_g t_s, \quad \gamma = E_m E_s t_m t_s,\\
&\delta = E_g E_s t_g t_m t_s,\\
&\Theta = \alpha t_g + \alpha t_m + \beta t_g + \beta t_s + 2\delta,\\
&\Phi = \alpha t_g^2 + \alpha t_m^2 + \beta t_g^2 + \beta t_s^2 + \gamma t_m^2 + \gamma t_s^2,\\
&\Psi = \alpha t_g t_m + \beta t_g t_s + \gamma t_m t_s.
\end{aligned} \tag{11}$$

The tip displacement of the laminate can be calculated from the curvature as

$$D = -\frac{1}{2}\kappa L^2. \tag{12}$$

It can be seen from (10) and (12) that tip displacement D depends on the magnetostriction, elastic properties, and thicknesses. Since λ_s is constant when the Galfenol layer is magnetically saturated, the tip displacement is determined only by the elastic parameters and the thicknesses.

In order to maximize the tip displacement, different elastic parameters and substrate thicknesses are investigated by employing (10) and (12). Since the total thickness of the composite beam is relatively small, the adhesive layer has to be taken into account in optimization. Previous work has neglected the effect of the adhesive layer (Gehring et al., 2000; Guerrero and Wetherhold, 2003).

Simulation results are shown in Figure 3 based on the proposed model (solid lines) and the model without considering the adhesive layer (dashed lines), for two different modulus ratios ($E_g/E_s = 1$ and $E_g/E_s = 5$). The thickness of the adhesive layer is 1/5th of the Galfenol layer. Comparison of panels (b) and (c) reveals that consideration of the adhesive layer yields reduced deflections due to the compliance of the adhesive.

Figure 3(a) shows that the displacement versus thickness ratio exhibits a peak. To the left of the peak, the deflection increases monotonically as the thickness of the substrate decreases. The opposite is true to the right of the peak. The reason for the peak has been explained physically by Gehring et al. (2000). For low thickness ratios, the active layer cannot effectively deform the substrate and little deflection is observed. At high thickness ratios, most of the deformation is a uniform longitudinal strain and little bending of the beam takes place. The existence of an optimum thickness ratio can be explained mathematically. Substitution of the stiffness ratio $\tilde{\alpha} \equiv t_g/t_s$ into (10) gives

$$\kappa = \frac{6\tilde{\alpha}^2 E_g t_g \lambda_s \left(E_m \tilde{\alpha}^2 t_m (t_g + t_m) + E_s t_g^2 (\tilde{\alpha} + 1) + 2E_s t_g t_m \tilde{\alpha}\right)}{\tilde{\alpha}^4 t_g^4 E_g^2 + t_g^4 E_s^2 + \tilde{\alpha}^4 t_m^4 E_m^2 + \chi}, \tag{13}$$

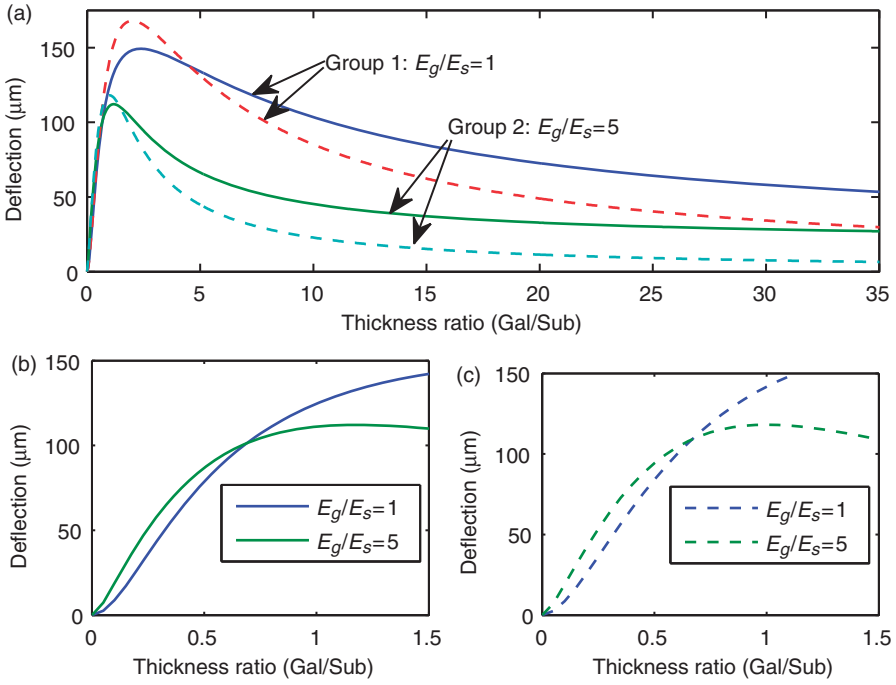

Figure 3. *(a) Deflection vs thickness ratio based on the proposed model (solid lines) and the model without considering the adhesive layer (dashed lines), for two different modulus ratios ($E_g/E_s = 1$ and $E_g/E_S = 5$). (b) Proposed model below the optimal thickness ratio. (c) Model without consideration of the adhesive layer, below the optimal thickness ratio.*

where

$$\chi = \tilde{\alpha}^4 E_g E_m t_g t_m \tilde{\epsilon} + \tilde{\alpha} E_g E_s t_g^4 \tilde{\eta} + 12\tilde{\alpha}^2 E_g E_s t_g t_m \tilde{\mu} + \tilde{\alpha} E_s E_m t_g t_m \tilde{\omega},$$
$$\tilde{\epsilon} = 4t_g^2 + 6t_g t_m + 4t_m^2, \quad \eta = 4\tilde{\alpha}^2 + 6\tilde{\alpha} + 4,$$
$$\tilde{\mu} = \tilde{\alpha} t_g^2 + \tilde{\alpha} t_g t_m + t_g^2, \quad \tilde{\omega} = 4\tilde{\alpha}^2 t_m^2 + 6\tilde{\alpha} t_g t_m + 4t_g^2.$$

Since t_g and t_m are constants, the solution to $d\kappa/d\tilde{\alpha} = 0$ gives the optimal thickness ratio as

$$\tilde{\alpha} = \left\{ \left[\left(\frac{\hat{\alpha}}{27\hat{\beta}^3} + \frac{E_s t_g^3}{\hat{\beta}} - \frac{\hat{\gamma}\hat{\alpha}}{6\hat{\beta}^2} \right)^2 - \left(\frac{\hat{\alpha}^2}{9\hat{\eta}^2} - \frac{\hat{\gamma}}{3\hat{\eta}} \right)^3 \right]^{1/2} - \frac{\hat{\alpha}^3}{27\hat{\beta}^3} - \frac{E_s t_g^3}{\hat{\beta}} + \frac{\hat{\gamma}\hat{\alpha}}{6\hat{\beta}^2} \right\}^{1/3} + \frac{\frac{\hat{\alpha}^2}{9\hat{\beta}^2} - \frac{\hat{\gamma}}{3\hat{\beta}}}{\left\{ \left[\left(\frac{\hat{\alpha}}{27\hat{\beta}^3} + \frac{E_s t_g^3}{\hat{\beta}} - \frac{\hat{\gamma}\hat{\alpha}}{6\hat{\beta}^2} \right)^2 - \left(\frac{\hat{\alpha}^2}{9\hat{\eta}^2} - \frac{\hat{\gamma}}{3\hat{\eta}} \right)^3 \right]^{1/2} - \frac{\hat{\alpha}^3}{27\hat{\beta}^3} - \frac{E_s t_g^3}{\hat{\beta}} + \frac{\hat{\gamma}\hat{\alpha}}{6\hat{\beta}^2} \right\}^{1/3} - \frac{\hat{\alpha}}{3\hat{\beta}}}, \tag{14}$$

where

$$\hat{\alpha} = 6E_m t_m t_g^2 + 6E_m t_g t_m^2, \quad \hat{\beta} = 3E_m t_g t_m^2 - E_g t_g^3 + 2E_m t_m^3,$$
$$\hat{\gamma} = 3E_s t_g^3 + 6E_s t_m t_g^2, \quad \hat{\eta} = -E_g t_g^3 + 3E_m t_g t_m^2 + 2E_m t_m^3.$$

The optimal thickness ratio for achieving peak deflection is higher when the substrate is stiff. Below this peak, softer substrates are more desirable for maximum deflection, as shown in Figure 3(b) and (c). This is because when the thickness of the substrate is large relative to the Galfenol layer, the combination of large thickness and large modulus makes the substrate more difficult to be actuated. Above the cross-over point, the active layer is driving a thin substrate and most of the deformation is a uniform longitudinal strain (Gehring et al., 2000). In order to achieve bending rather than longitudinal deformation, a stiff substrate is necessary.

Experimental verification of the model predictions is conducted on seven specimens with various thicknesses. The substrate material is stainless steel, which has a higher elastic modulus than other typical substrate materials such as brass or aluminum. Sample details are provided in Table 1. Experimental measurements are compared against model simulations in Figure 4. Due to a limit on available stainless steel thickness, the largest ratio tested was 15:1. Consideration of the adhesive layer yields a significant improvement over the model without adhesive layer. The optimal thickness ratio is around 4 according to simulation and experimental results. Since the thickness of the Galfenol layer is constant, a high thickness ratio implies a thin substrate. At high thickness ratios, the adhesive layer can be taken as an equivalent substrate, making the substrate layer stiffer than the model without adhesive. Over most of the range of thickness ratios a stiffer substrate will give higher deflection. This is why in Figure 4 the proposed model predicts higher deflection above a thickness ratio of 12 than the model without adhesive.

DYNAMIC BEAM MODEL

When Galfenol is bonded to a non-magnetic material, the constraint of the substrate causes bending of the beam. With steel-like ductility and stiffness, Galfenol bends along with the substrate. To describe the dynamic response of the active composite beam driven by

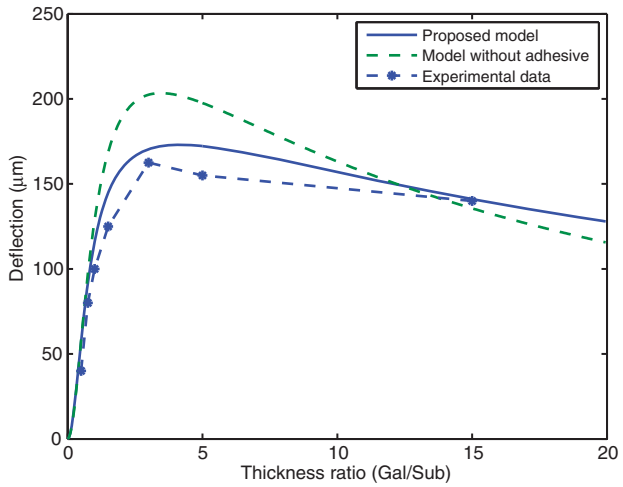

Figure 4. *Comparison of experimental data and models with and without consideration of the adhesive layer.*

Table 1. Geometric details of the beams used for model verification.

Sample	I	II	III	IV	V	VI	VII
Substrate thickness (mm)	0.762	0.508	0.381	0.254	0.127	0.0762	0.0254
Thickness ratio (Gal/Sub)	1:2	3:4	1:1	1.5 :1	3:1	5:1	15:1

The length of the beam is 25 mm, the width is 6.35 mm, and the thickness of the Galfenol layer is 0.381 mm.

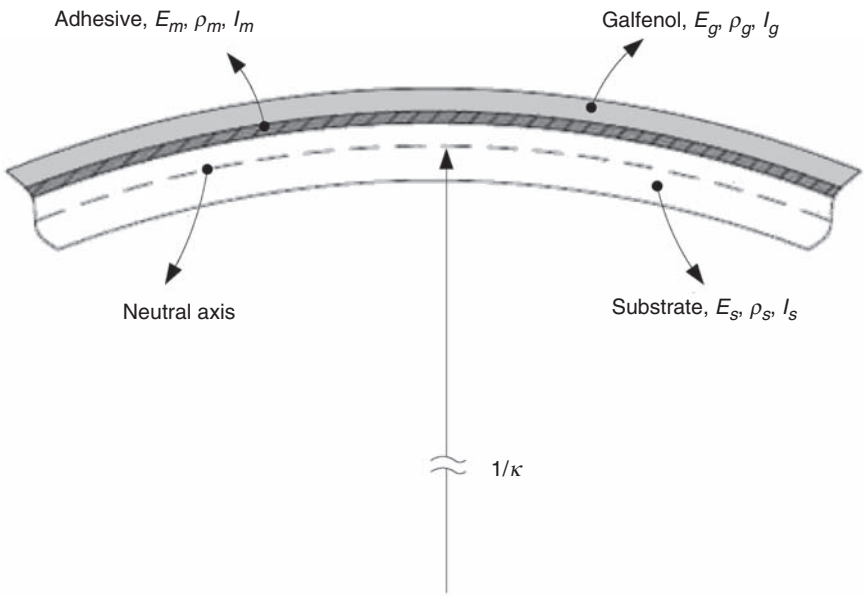

Figure 5. *Schematic representation of the composite beam subjected to bending.*

Galfenol, a dynamic model is formulated and subsequently implemented with finite-element spatial discretization and Newmark temporal integration.

Governing Equation

Deformation of the composite beam is illustrated in Figure 5 along with the corresponding parameters of each layer, including elastic modulus E, mass density ρ, and moment of inertia I.

The total bending moment is calculated by integrating the differential moment due to stress over the cross-sectional area:

$$\begin{aligned} M &= -\int_{A_g} E_g(\kappa z + \lambda) z \mathrm{d}A_g - \int_{A_s} E_s \kappa z^2 \mathrm{d}A_s \\ &\quad - \int_{A_m} E_m \kappa z^2 \mathrm{d}A_m \\ &= -\kappa(E_s I_s + E_m I_m + E_g I_g) - E_g A_g \lambda (h - t_g/2) \\ &= (E_s I_s + E_m I_m + E_g I_g)\frac{\partial^2 w(x,t)}{\partial x^2} - E_g A_g \lambda (h - t_g/2). \end{aligned} \tag{15}$$

The total shear force Q is

$$\begin{aligned} Q = \frac{\partial M}{\partial x} &= (E_s I_s + E_m I_m + E_g I_g)\frac{\partial^3 w(x,t)}{\partial x^3} \\ &\quad - E_g A_g (h - t_g/2)\frac{\partial \lambda}{\partial x}, \end{aligned} \tag{16}$$

where $w(x, t)$ is the vertical deflection of the neutral plane. From (9), the distance from the top of the beam to the neutral axis h is dependent on curvature κ and saturation magnetostriction λ_S. The curvature κ can be calculated as (Wetherhold and Chopra, 2001),

$$\kappa = \frac{AM^{\lambda} - BN^{\lambda}}{AD - B^2}, \tag{17}$$

where A, B, and D are the extensional, coupling, and bending stiffnesses:

$$\begin{aligned} A &= \sum_{i=1}^{N} Q_i t_i, \\ B &= \frac{1}{2}\sum_{i=1}^{N} Q_i (h_i^2 - h_{i-1}^2), \\ D &= \frac{1}{3}\sum_{i=1}^{N} Q_i (h_i^3 - h_{i-1}^3), \end{aligned} \tag{18}$$

where N denotes the number of layers in the laminate, Q_i is the x-direction stiffness for the i-th layer, and h_i the distance of the i-th layer from the mid-surface.

Wetherhold and Chopra (2001) also provide expressions for the equivalent actuation moment and force per unit length,

$$\begin{aligned} N^{\lambda} &= \sum_{i=1}^{N} Q_i t_i \lambda_i, \\ M^{\lambda} &= \frac{1}{2}\sum_{i=1}^{N} Q_i (h_i^2 - h_{i-1}^2)\lambda_i. \end{aligned} \tag{19}$$

Since Galfenol is biased during normal operation and experimental characterization, the biased magnetostriction λ_b is used in (15) and (19).

Force balancing on a generic cross-section of the beam gives

$$(\rho_g A_g + \rho_s A_s + \rho_m A_m)\frac{\partial^2 w(x,t)}{\partial t^2} + \hat{c}\frac{\partial w(x,t)}{\partial t} + \frac{\partial Q}{\partial x} = 0, \tag{20}$$

where ĉ is the damping constant. A Rayleigh-type damping is employed by assuming that energy dissipation in the system is proportional to velocity. The generalized velocity is the only relevant state variable that affects the damping force. Energy dissipation due to eddy current has been ignored since the main flux path is laminated, consistent with best design practices for this type of actuator. Substitution of (16) into this expression gives

$$\begin{aligned}(\rho_g A_g + \rho_s A_s + \rho_m A_m)\frac{\partial^2 w(x,t)}{\partial t^2} + \hat{c}\frac{\partial w(x,t)}{\partial t} \\ + \frac{\partial}{\partial x}((E_s I_s + E_m I_m + E_g I_g)\frac{\partial^3 w(x,t)}{\partial x^3} \\ - E_g A_g (h - t_g/2)\frac{\partial \lambda}{\partial x}) = 0.\end{aligned} \tag{21}$$

For convenience, the following definitions are used:

$$\begin{aligned} EI &\equiv E_s I_s + E_m I_m + E_g I_g, \\ \hat{H} &\equiv E_g A_g (h - t_g/2), \\ \rho A &\equiv \rho_g A_g + \rho_s A_s + \rho_m A_m. \end{aligned} \tag{22}$$

The governing equation of the composite beam can now be expressed as

$$EI\frac{\partial^4 w(x,t)}{\partial x^4} + \hat{c}\frac{\partial w(x,t)}{\partial t} + \rho A\frac{\partial^2 w(x,t)}{\partial t^2} = \hat{H}\frac{\partial^2 \lambda}{\partial x^2}. \tag{23}$$

Discretization and Weak Form

To arrive at a weak form of (23), the space of test functions is defined as

$$V = H^2(0,L) \equiv \left\{ v \in H^2(0,L) | v(0) = \frac{\partial v(0)}{\partial x} = 0 \right\}. \tag{24}$$

Multiplication by test functions followed by integration yields the weak form:

$$\begin{aligned}\int_0^L (EI\frac{\partial^4 w(x,t)}{\partial x^4} + \hat{c}\frac{\partial w(x,t)}{\partial t} + \rho A\frac{\partial^2 w(x,t)}{\partial t^2}) v \mathrm{d}x \\ = \int_0^L \hat{H}\frac{\partial^2 \lambda}{\partial x^2} v \mathrm{d}x,\end{aligned} \tag{25}$$

for all $v \in V$. To approximate (25), the Galerkin method is employed over finite elements where the test functions have the same basis as w. The domain of the composite beam is divided into N elements, each having two nodes as shown in Figure 6(a). Each node has two degrees of freedom, vertical deflection w and rotation θ, Figure 6(b).

For small rotations, the bending angle θ is equal to the slope of the vertical displacement w with respect to x. The primary variables to be solved for can be expressed as

$$w^e = [w_1 \quad \frac{\mathrm{d}w_1}{\mathrm{d}x} \quad w_2 \quad \frac{\mathrm{d}w_2}{\mathrm{d}x}]. \tag{26}$$

For a typical element $\Omega_e = (x_e,\ x_{e+1})$, integration over the element of the fourth derivative term by parts in (25) gives

$$\begin{aligned}&\int_{x_e}^{x_{e+1}} (EI\frac{\partial^2 w(x,t)}{\partial x^2}\frac{\partial^2 v(x)}{\partial x^2} + \hat{c}\frac{\partial w(x,t)}{\partial t} v(x) + \rho A\frac{\partial^2 w(x,t)}{\partial t^2}) v \mathrm{d}x \\ &= \int_{x_e}^{x_{e+1}} \hat{H}\frac{\partial^2 \lambda}{\partial x^2} v(x) \mathrm{d}x + (v(x) Q_q^e)_{x_e} - (\frac{\mathrm{d}v(x)}{\mathrm{d}x} Q_m^e)_{x_e} \\ &- (v(x) Q_q^e)_{x_{e+1}} + (\frac{\mathrm{d}v(x)}{\mathrm{d}x} Q_m^e)_{x_{e+1}},\end{aligned} \tag{27}$$

where

$$\begin{aligned} Q_q^e &= EI\frac{\partial^3 w(x,t)}{\partial x^3}, \\ Q_m^e &= EI\frac{\partial^2 w(x,t)}{\partial x^2}. \end{aligned} \tag{28}$$

The solution $w(x, t)$ of (27) is approximated by expressions of the form

$$w(x, t_s) = \sum_j^n w_j^e(t_s)\phi_j^e(x), \tag{29}$$

where $w_j^e(t_s)$ is the value of $w(x, t)$ at time t_s and node j of the element Ω_e; $\phi_j^e(x)$ is an interpolation function. Here, the Hermite cubic interpolation functions are used (see Reddy (1993) for details).

Substitution of (29) and $v(x) = \phi_i(x)$ into (27) gives the second-order finite element model

$$[M]\{\ddot{w}\} + [C]\{\dot{w}\} + [K]\{w\} = \{F\} + \{F_{BCs}\}, \tag{30}$$

where

$$\begin{aligned} M_{ij} &= \int_{x_e}^{x_{e+1}} (\rho A \phi_i \phi_j) \mathrm{d}x, \\ C_{ij} &= \int_{x_e}^{x_{e+1}} \hat{c}\phi_i \phi_j \mathrm{d}x, \\ K_{ij} &= \int_{x_e}^{x_{e+1}} (EI\frac{\partial^2 \phi_i}{\partial x^2}\frac{\partial^2 \phi_j}{\partial x^2}) \mathrm{d}x, \end{aligned}$$

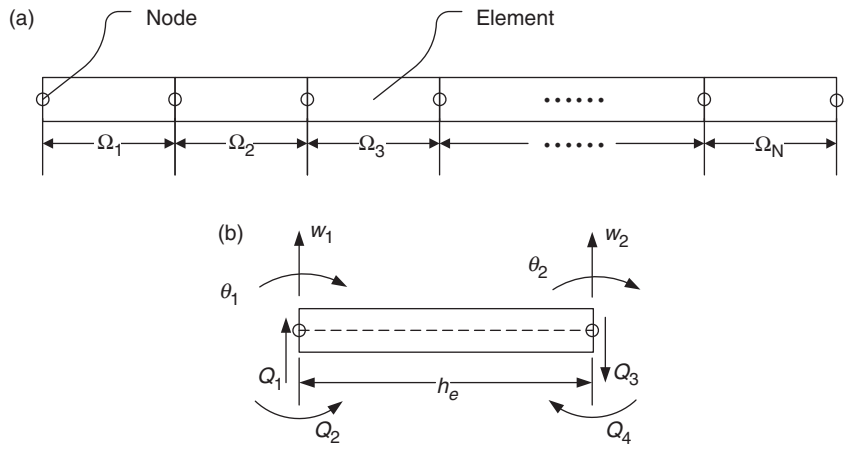

Figure 6. *(a) Discretization of the beam; (b) degrees of freedom of an element.*

$$F_i = \int_{x_e}^{x_{e+1}} \hat{H}\frac{\partial^2 \lambda}{\partial x^2}\phi_i \mathrm{d}x,$$
$$\{F_{BCs}\} = \left[\frac{\mathrm{d}}{\mathrm{d}x}(\hat{H}\lambda)|_{x_e} \quad -\hat{H}\lambda|_{x_e} \quad -\frac{\mathrm{d}}{\mathrm{d}x}(\hat{H}\lambda)|_{x_{e+1}} \quad \hat{H}\lambda|_{x_{e+1}}\right]^T. \tag{31}$$

Equation (30) shows the actuation model of the composite beam, in which the load vector is a function of boundary conditions and the magnetostriction of the Galfenol layer. In order to relate tip displacement with the drive current, a current–magnetostriction relationship is needed. A linear relationship is assumed which has the form

$$\lambda = d_g H = d_g N_c I_c, \tag{32}$$

where N_c is the number of turns per unit length in the coil, d_g the piezomagnetic coefficient, H the magnetic field, and I_c denotes current.

Combination of (30) and (32) gives the dynamic response of the composite beam to drive currents. We assume the magnetic field is uniform along the cantilever and through its thickness, hence the derivative terms of magnetostriction are zero in (30).

Solution and Validation

Newmark integration (Zhou and Zhou, 2007) is employed to solve the actuation model (30), which is expressed as

$$\{w\}_{t+\Delta t} = [\hat{K}]^{-1}\{\hat{F}\}, \tag{33}$$

where

$$[\hat{K}] = [K] + \alpha_0[M] + \alpha_1[C], \tag{34}$$

$$\begin{aligned}\{\hat{F}\} = \{\hat{F}\}_{t+\Delta t} &+ [M](\alpha_0\{w\}_t + \alpha_2\{\dot{w}\}_t + \alpha_3\{\ddot{w}\}_t) \\ &+ [C](\alpha_1\{w\}_t + \alpha_4\{\dot{w}\}_t + \alpha_5\{\ddot{w}\}_t),\end{aligned} \tag{35}$$

and $[C]$ is the damping matrix. Velocity and acceleration are involved in (35) and they are calculated as

$$\begin{aligned}\{\ddot{w}\}_{t+\Delta t} &= \alpha_0(\{w\}_{t+\Delta t} + \{w\}_t) - \alpha_2\{\dot{w}\}_t - \alpha_3\{\ddot{w}\}_t, \\ \{\dot{w}\}_{t+\Delta t} &= \{\dot{w}\}_t + \alpha_6\{\ddot{w}\}_t + \alpha_7\{\ddot{w}\}_{t+\Delta t}.\end{aligned} \tag{36}$$

The parameters involved in Newmark integration are:

$$\begin{aligned}&\alpha_0 = \frac{1}{\beta\Delta t^2},\ \alpha_1 = \frac{\gamma}{\beta\Delta t},\ \alpha_2 = \frac{1}{\beta\Delta t},\ \alpha_3 = \frac{1}{2\beta} - 1, \\ &\alpha_4 = \frac{\gamma}{\beta} - 1,\ \alpha_5 = \frac{\Delta t}{2}\left(\frac{\gamma}{\beta} - 2\right),\ \alpha_6 = \Delta(1-\gamma), \\ &\alpha_7 = \Delta t\gamma,\ \beta = 0.25,\ \gamma = 0.5.\end{aligned} \tag{37}$$

The initial conditions of the beam required in (36) are known and the dynamic response of the composite beam is calculated from expressions (33) to (37).

The structural damping is modeled as Rayleigh damping in which the damping matrix is formed by the linear combination of mass and stiffness matrices (Kiral, 2008):

$$[C] = c_0[M] + c_1[K]. \tag{38}$$

Rayleigh damping coefficients c_0 and c_1 can be evaluated from damping ratios ζ_m and ζ_n, which are associated with two specific fundamental frequencies ω_m and ω_n (Clough and Penzien, 1993):

$$\begin{Bmatrix} c_0 \\ c_1 \end{Bmatrix} = \frac{2\omega_m\omega_n}{\omega_m^2\omega_n^2}\begin{bmatrix} \omega_n & -\omega_m \\ -1/\omega_n & 1/\omega_m \end{bmatrix}\begin{Bmatrix} \zeta_m \\ \zeta_n \end{Bmatrix}. \tag{39}$$

The damping ratio is identified from the impulse-response test shown in Figure 7. This analysis gives $\zeta = 0.0056$. The damping ratios ζ_m and ζ_n are assumed equal.

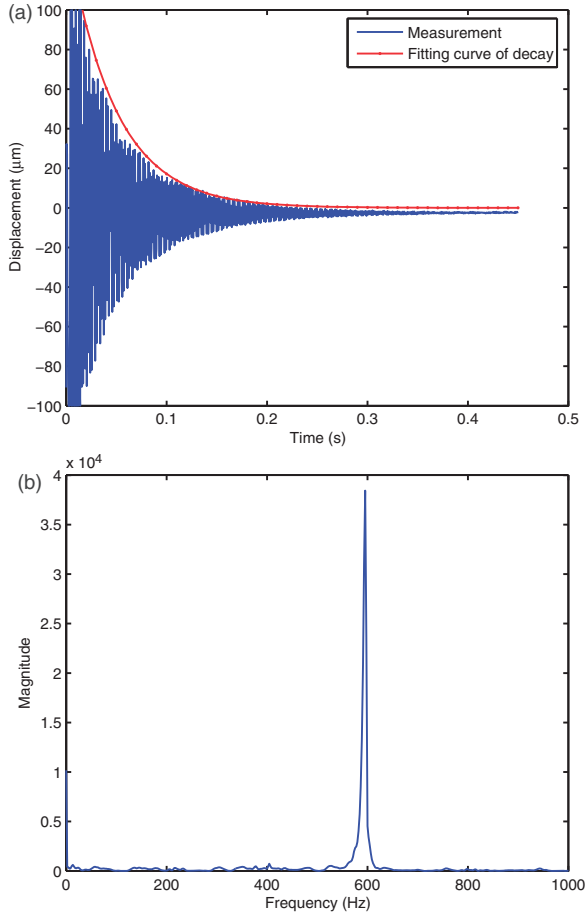

Figure 7. *(a) Impulse response of the composite beam; (b) FFT of the impulse response.*

EXPERIMENTS AND DISCUSSION

Experimental Setup

The experimental configuration is illustrated in Figure 8, in which dSpace ControlDesk is used for real-time manipulation; the tip displacement is measured with a laser sensor. The cantilever is clamped in a metglas, U-shaped laminated frame and the driving coil is wound on the frame. The thickness of the Galfenol layer is 0.381 mm and the thickness of the epoxy layer is 1/5th of the Galfenol layer. The thickness ratio is chosen as 3:1, which is as close as practically possible to the optimal ratio in Figure 4. The sampling frequency in the dSpace system is 6000 Hz whereas the sampling rate in the laser sensor is 20 μs. Both cause frequency-independent pure time delay in the measurements, equivalent to 0.1867 ms. This delay is added into the dynamic model when it is excited with the magnetic field.

Discussion

Model validation is conducted at different frequencies ranging from 10 to 320 Hz, as illustrated in Figures 9 and 10. Tip displacement and actuation current relationships for representative frequencies are shown in Figure 11.

To quantify the maximum value of predictive error, the following definition is utilized:

$$\text{Ratio} \equiv \frac{d_{pk} - m_{pk}}{d_{pk}} \times 100\%, \tag{40}$$

where m_{pk} denotes the peak to peak value of the steady-state model solution while d_{pk} denotes the corresponding peak to peak value of the measurement. The values of Ratio are presented within each figure. The RMS

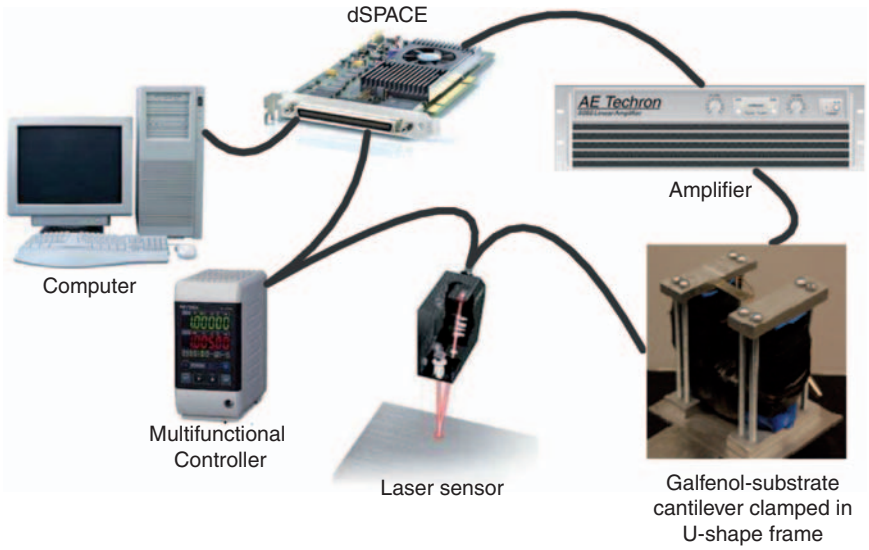

Figure 8. *Schematic of the experimental setup.*

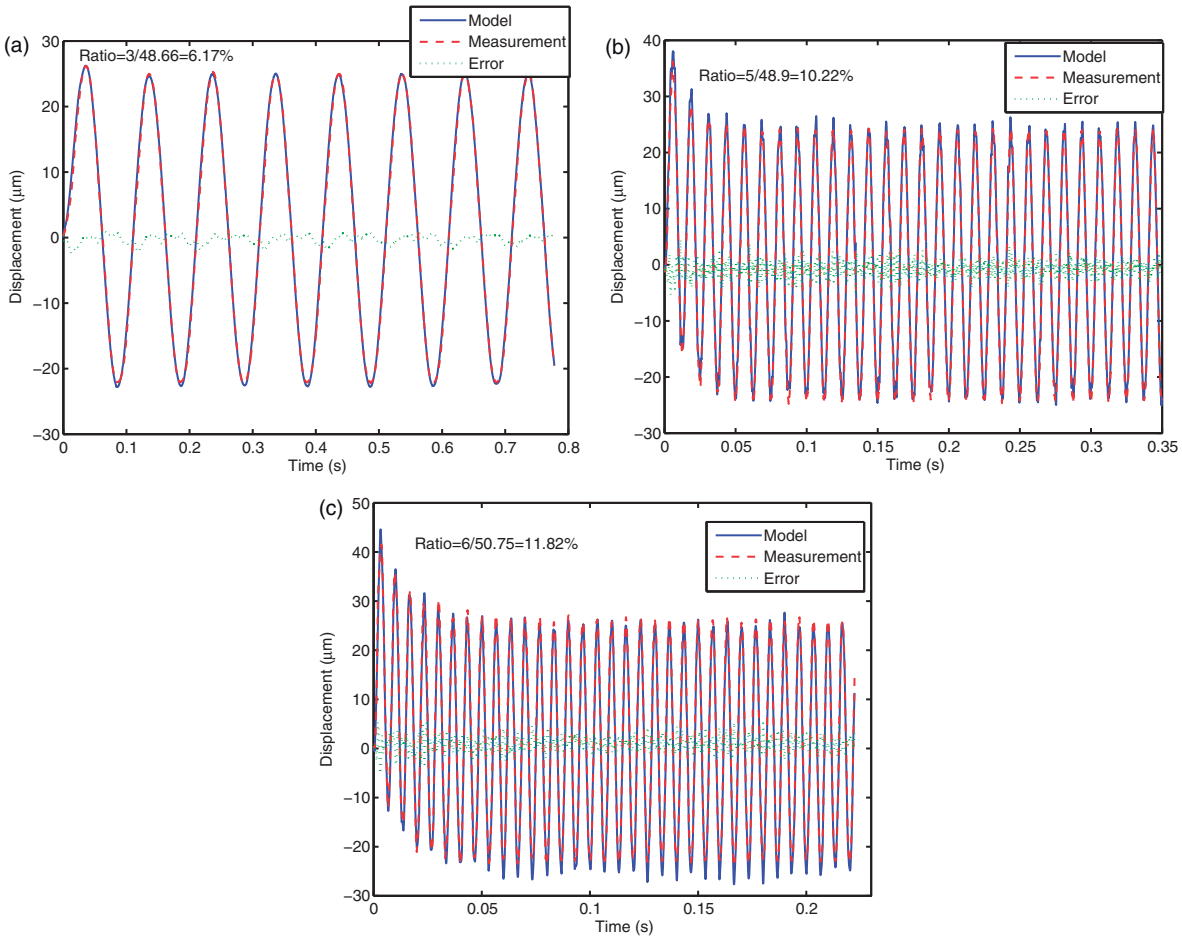

Figure 9. *Model validation at different dynamic frequencies, (a) 10 Hz; (b) 80 Hz; (c) 150 Hz.*

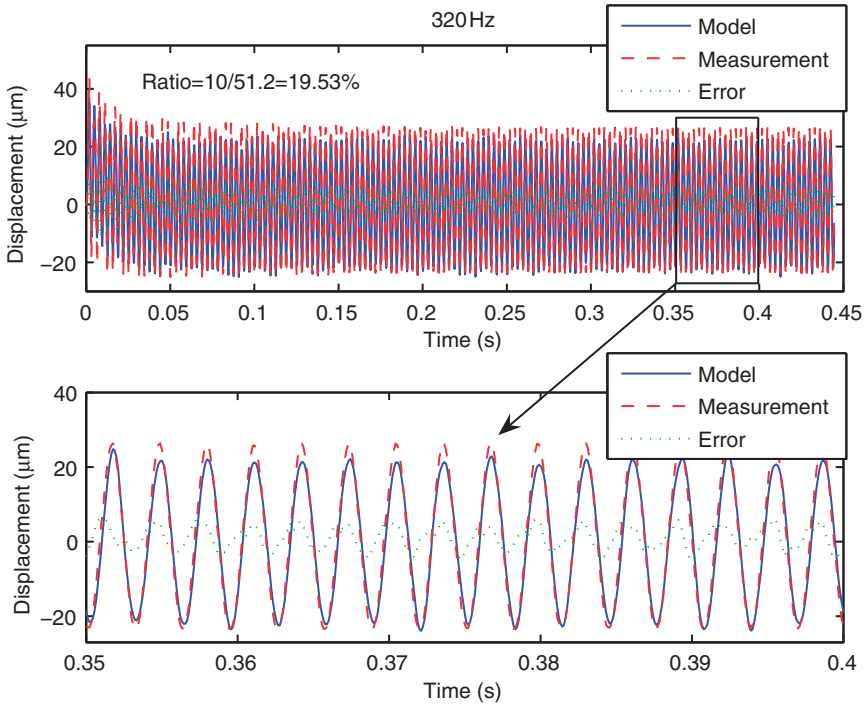

Figure 10. *Model validation at 320 Hz.*

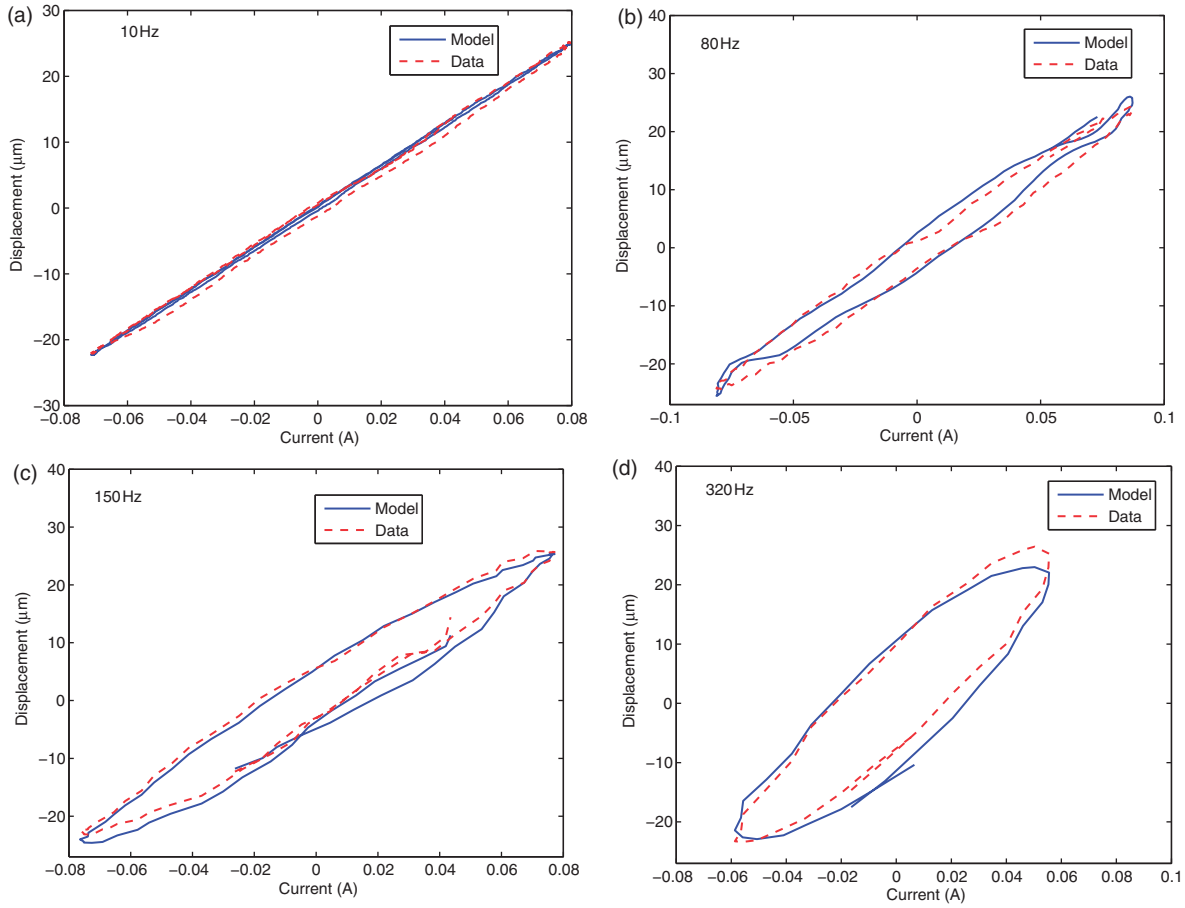

Figure 11. *Tip displacement vs applied current at varied actuation frequencies, (a) 10 Hz; (b) 80 Hz; (c) 150 Hz; (d) 320 Hz.*

Table 2. Comparison of experiments at different frequencies.

Input frequency (Hz)	Measurement (μm)	RMS value of error (μm)	Error (%)
10	48.66	0.7012	1.44
30	47.17	0.8569	1.82
50	49.75	0.9011	1.81
80	48.9	1.2499	2.56
120	49.61	1.1343	2.29
150	50.75	1.6399	3.23
200	55.04	1.8932	3.44
250	48.85	2.2097	4.52
320	51.2	3.2442	6.34

value of the modeling error is presented in Table 2. In order to scale this error, the corresponding error ratio is defined as $\text{Error} = \text{RMS}(d_d - m_d)/d_{pk} \times 100\%$, where d_d denotes the measurement signal and m_d denotes the signal generated by the model. The values of Error are presented in the last column of Table 2.

The dynamic model accurately describes both the transient and steady-state responses of the composite beam. The RMS error between the model and experimental data ranges between 1.44% at 10 Hz and 6.34% at 320 Hz. The increase in error with increasing frequency is likely due to eddy current losses, which are not accounted for in the model. It is emphasized that the model parameters were identified from quasistatic measurements conducted at 1 Hz, and the same set of parameters was employed across the frequency range. We justify the use of linear piezomagnetic modeling in that the Galfenol unimorph is biased with a DC current

and operated in a relatively linear regime. Galfenol exhibits significantly less hysteresis than Terfenol-D and other active materials.

CONCLUDING REMARKS

The steel-like structural properties of Galfenol make this material attractive for composite unimorph beam micro-positioners. The adhesive layer is shown to reduce tip deflection, and the effect of this layer is taken into account for optimal design of the unimorph. A dynamic model is presented which quantifies the electromechanical response of the beam in transient or steady-state conditions. The use of linear piezomagnetic equations is justified in that Galfenol exhibits relatively low hysteresis loss, especially when magnetically biased. The field is assumed to be uniform along the length of the beam, rotary inertias are ignored, and damping is assumed to be frequency independent. Dynamic losses due to eddy currents are ignored under the assumption that the laminated construction of the composite beam reduces dynamic losses. That being said, the measurements do show an increase in dynamic losses with increasing frequency. These losses will be quantified in a future study. Despite these assumptions and limitations, the linear model is extremely accurate without the need for adjustable parameters over the frequency range being considered. The relative simplicity of the model is beneficial for design and control purposes.

ACKNOWLEDGMENT

The authors acknowledge the financial support provided by the National Natural Science Foundation of China (Grant No. 50865008), Ph.D. Programs Foundation of Ministry of Education of China (Grant No. 20090143110005) and the China Scholarship Council. The authors also acknowledge Julie Slaughter of Etrema Products, Inc. for providing the Galfenol samples utilized in this study.

REFERENCES

Baillargeon, B.P. and Vel, S.S. 2005. "Active Vibration Suppression of Sandwich Beams using Piezoelectric Shear Actuators: Experiments and Numerical Simulations," *Journal of Intelligent Material Systems and Structures*, 16:517–530.

Basantkumar, R.R., Stadler, B.J., Robbins, W.P. and Summers, E. 2006. "Integration of Thin-Film Galfenol with MEMS Cantilevers for Magnetic Actuation," *IEEE Transactions on Magnetics*, 42:3102–3104.

Bashash, S., Jalili, N., Evans, P.G. and Dapino, M.J. 2009. "Recursive Memory-based Hysteresis Modeling for Solid-state Smart Actuators," *Journal of Intelligent Material Systems and Structures*, 20:2161–2171.

Chen, X. 2004. "Optimization of a Cantilever Microswitch with Piezoelectric Actuation," *Journal of Intelligent Material Systems and Structures*, 15:823–834.

Clough, R.W. and Penzien, J. 1993. *Dynamics of Structures*, McGraw-Hill, Inc., New York.

Dapino, M.J., Smith, R.C. and Flatau, A.B. 2000. "Structural-Magnetic Strain Model for Magnetostrictive Transducers," *IEEE Transactions on Magnetics*, 36:545–556.

Datta, S., Atulasimha, J., Mudivarthi, C. and Flatau, A.B. 2008. "The Modeling of Magnetomechanical Sensors in Laminated Structures," *Smart Materials and Structures*, 17:1–9.

Datta, S., Atulasimha, J., Mudivarthi, C. and Flatau, A.B. 2009. "Modeling of Magnetomechanical Actuators in Laminated Structures," *Journal of Intelligent Material Systems and Structures*, 20:1121–1135.

Downey, P.R. and Flatau, A.B. 2005. "Magnetoelastic Bending of Galfenol for Sensor Applications," *Journal of Applied Physics*, 97:1–3.

du Trémolet de Lacheisserie, E. and Peuzin, J.C. 1994. "Magnetostriction and Internal Stresses in Thin Films: The Cantilever Method Revisited," *Journal of Magnetism and Magnetic Materials*, 136:189–196.

Evans, P.G. and Dapino, M.J. 2008. "State-Space Constitutive Model for Magnetization and Magnetostriction of Galfenol Alloys," *IEEE Transactions on Magnetics*, 44:1711–1720.

Gehring, G.A., Cooke, M.D., Gregory, I.S., Karl, W.J. and Watts, R. 2000. "Cantilever Unified Theory and Optimization for Sensors and Actuators," *Smart Materials and Structures*, 9:918–931.

Guerrero, V.H. and Wetherhold, R.C. 2003. "Magnetostrictive Bending of Cantilever Beams and Plates," *Journal of Applied Physics*, 94:6659–6666.

Kim, S.J. and Jones, J.D. 1995. "Influence of piezo-actuator thickness on the active vibration control of a cantilever beam," *Journal of Intelligent Material Systems and Structures*, 6:610–623.

Kiral, Z. 2008. "Damped Response of Symmetric Laminated Composite Beams to Moving Load with Different Boundary Conditions," *Journal of Reinforced Plastics and Composites*, 28:2511–2526.

Krishnamurthy, A.V. 1999. "Sensing of Delaminations in Composite Laminates Using Embedded Magnetostrictive Particle Layers," *Journal of Intelligent Material Systems and Structures*, 10:825–835.

Kumar, J.S., Ganesan, N., Swarnamani, S. and Padmanabhan, C. 2003. "Active Control of Beam with Magnetostrictive Layer," *Computers and Structures*, 81:1375–1382.

Lee, H.S. and Cho, C. 2008. "Study on Advanced Multilayered Magnetostrictive Thin Film Coating Techniques for MEMS Application," *Journal of Materials Processing Technology*, 201:678–682.

Reddy, J.N. 1993. *An Introduction to the Finite Element Method*, McGraw-Hill, Inc., New York.

Suhariyono, A., Goo, N.S. and Park, H.C. 2008. "Use of Lightweight Piezo-Composite Actuators to Surpress the Free Vibration of an Aluminum Beam," *Journal of Intelligent Material Systems and Structures*, 19:101–112.

Sun, C.T. and Zhang, X.D. 1995. "Use of Thickness-Shear Mode in Adaptive Sandwich Structures," *Smart Materials and Structures*, 4:202–206.

Ueno, T. and Higuchi, T. 2007. "Magnetostrictive Bending Micro Actuator Using Iron Gallium Alloy," In: *Proceedings of SPIE, the International Society for Optical Engineering*, Vol. 6526, San Diego, California.

Wang, Y.Z., Atulasimha, J., Clarke, J. and Sundaresan, V.B. 2010. "Thickness Ratio Effects on Quasistatic Actuation and Sensing Behavior of Laminate Magnetoelectric Cantilevers," In: *Proceedings of SPIE, the International Society for Optical Engineering*, Vol. 7644, San Diego, California.

Wetherhold, R.C. and Chopra, H.D. 2001. "Beam Model for Calculating Magnetostriction Strains in Thin Films and Multilayers," *Applied Physics Letters*, 79:3818–3820.

Yan, W., Cai, J.B. and Chen, W.Q. 2009. "Analytical Modeling and Static Response of a Curved Beam with Imperfectly Bonded Piezoelectric

Actuators," In: *Joint Conference of the 2009 Symposium on Piezoelectricity, Acoustic Waves, and Device Applications*, China.

Zabihollah, A., Sedagahti, R. and Ganesan, R. 2007. "Active Vibration Suppression of Smart Laminated Beams Using Layerwise Theory and an Optimal Control Strategy," *Smart Materials and Structures*, 16:2190–2201.

Zhou, H.M. and Zhou, Y.H. 2007. "Vibration Suppression of Laminated Composite Beams Using Actuators of Giant Magnetostrictive Materials," *Smart Materials and Structures*, 16:198–206.